

EFFECT OF SOLUTION TREATMENT ON HIGH TEMPERATURE  
OXIDATION OF Fe-33Ni-19Cr AND Fe-40Ni-24Cr ALLOYS

NORAZIANA BINTI PARIMIN

A thesis submitted in fulfilment of the  
requirements for the award of the degree of  
Doctor of Philosophy (Mechanical Engineering)

Faculty of Mechanical Engineering  
Universiti Teknologi Malaysia

MARCH 2015

*Specially dedicate to my beloved husband Mr Muhamad Safwan, my daughter Nuha Safiya, my parents Haji Parimin and Hajah Hasimah, my mother in law Hajah Salmah and also my sister Norilah. Thank you for all the everlasting love, boundless understanding, undying encouragement, and endless support.*

## ACKNOWLEDGEMENT

Praise be to Allah, the Most Gracious and Most Merciful for the completion of this research. For without His blessings, this study would surely not stick to its rail.

Foremost, I would like to express my deep gratitude to Professor Dr. Esah Hamzah, my research supervisor, for the continuous support of my Ph.D study and research, for her patient guidance, enthusiastic encouragement, immense knowledge and useful critiques of this research work. I could not have imagined having a better advisor and mentor for my Ph.D study.

I would also like to express my very great appreciation to Associate Professor Dr. Astuty Amrin, my research co-supervisor, for her motivation, valuable and constructive suggestions during the planning and development of this research work. Her willingness to give her time so generously has been very much appreciated.

I would also like to extend my thanks to all the members of staff at Faculty of Mechanical Engineering, Universiti Teknologi Malaysia, especially to the technicians of the Materials Science laboratory, Mr Adnan, Mr Azri, Mr Jeffry, Mr Ayup, Mr Amir and Mrs Farah for their help and assistance in running the experiment. My grateful thanks are also extended to Mr Hadzrul, Mr Azmi and Mr Nasir and all the members of staff at School of Materials Engineering, Universiti Malaysia Perlis who helped me in my research work.

I am particularly grateful for the assistance given by my fellow lab mates: Kurnia, Asma, Maureen, Yong and Intan, for the stimulating discussion and for all the joy we have had in the last four years, who also experienced all of the ups and downs of my research. I am indebted to them for their help.

I would like to thank the Universiti Malaysia Perlis and Ministry of Education Malaysia for providing the scholarship which allowed me to undertake this research.

Finally, I must express my gratitude to my husband Mr Muhamad Safwan and my daughter Nuha Safiya, for their love, support and encouragement throughout my study. My heartfelt thanks are extended to my parents Haji Parimin and Hajah Hasimah, my mother in law Hajah Salmah and my sisters and brothers, for their everlasting love and inspiration in my education. Last but not least, I wish to acknowledge the help provided by my sister Mrs Norilah for her patience, understanding and endless support.

## ABSTRACT

Nickel-based superalloys have the ability to form protective surface oxide scales at high temperature that provides them with resistance against further high temperature oxidation. In this research two types of nickel-based alloys namely, Fe-33Ni-19Cr and Fe-40Ni-24Cr were solution treated to vary the austenite grain size in order to observe its effect on the oxidation properties. The alloys were heat treated at temperatures of 950°C, 1000°C, 1050°C, 1100°C, 1150°C and 1200°C for 3 hours followed by water quench. The untreated and heat treated alloys were then subjected to high temperature oxidation under isothermal and cyclic condition for 500 hours and 150 cycles respectively in a specially designed oxidation rig. Thermogravimetric analysis in high purity oxygen was also performed on the alloys. The alloys were then analysed using optical microscope, scanning electron microscope, energy dispersive spectrometer and X-ray diffractometer. The results show that the oxide scales formed consist of various metal-based oxides with thickness of 1  $\mu\text{m}$  to 10  $\mu\text{m}$ . Both alloys show parabolic growth indicating the oxide was formed based on diffusion-controlled mechanism. It was found that the heat treatment processes at 950°C, 1000°C and 1050°C produced fine austenite grains of 55 – 61  $\mu\text{m}$  for Fe-33Ni-19Cr and 27 – 33  $\mu\text{m}$  for Fe-40Ni-24Cr alloys. Alloys treated at 1100°C, 1150°C and 1200°C produced coarse austenite grains of 65 – 100  $\mu\text{m}$  for Fe-33Ni-19Cr and 36 – 41  $\mu\text{m}$  for Fe-40Ni-24Cr alloys. Both alloys with fine austenite grains exhibited lower oxidation rate in isothermal and cyclic oxidation tests. This is due to the availability of ion diffusion path within the grain boundaries of fine grain alloys and hence allows the rapid formation of the protective oxide layer. Therefore, these alloys can be used for high temperature applications.

## ABSTRAK

Superaloi berasaskan nikel mempunyai kebolehan untuk membentuk lapisan perlindungan oksida permukaan pada suhu tinggi yang memberikan rintangan kepada pengoksidaan suhu tinggi. Di dalam kajian ini dua jenis aloi berasaskan nikel iaitu, Fe-33Ni-19Cr dan Fe-40Ni-24Cr telah dirawat larutan untuk membezakan saiz bijian austenit supaya dapat dilihat kesannya kepada sifat pengoksidaan. Kedua-dua aloi telah dirawat haba pada suhu 950°C, 1000°C, 1050°C, 1100°C, 1150°C dan 1200°C selama 3 jam diikuti dengan lindap kejut di dalam air. Aloi yang tidak dirawat dan dirawat haba telah melalui ujikaji pengoksidaan pada suhu tinggi di bawah keadaan sesuhu selama 500 jam dan berkitar untuk 150 kitaran dengan menggunakan rig pengoksidaan yang direka khas. Analisis termogravimetri dalam oksigen tulen telah juga dijalankan ke atas aloi tersebut. Aloi tersebut kemudian telah dianalisis dengan menggunakan mikroskop optik, mikroskop imbasan elektron, spektrometer serakan tenaga dan pembelau sinar-X. Keputusan kajian menunjukkan bahawa oksida yang terbentuk mengandungi pelbagai oksida berasaskan logam dengan ketebalan 1 µm hingga 10 µm. Kedua-dua aloi menunjukkan pertumbuhan parabolik menandakan oksida yang terbentuk adalah berdasarkan mekanisma resapan terkawal. Hasil kajian menunjukkan proses rawatan haba pada suhu 950°C, 1000°C dan 1050°C telah menghasilkan saiz bijian austenit yang halus dengan saiz 55 – 61 µm bagi aloi Fe-33Ni-19Cr dan 27 – 33 µm bagi aloi Fe-40Ni-24Cr. Aloi yang dirawat haba pada suhu 1100°C, 1150°C dan 1200°C menghasilkan saiz austenit yang kasar dengan saiz 65 – 100 µm bagi aloi Fe-33Ni-19Cr dan 36 – 41 µm bagi aloi Fe-40Ni-24Cr. Kedua-dua aloi yang mempunyai austenit berbijian halus menunjukkan kadar pengoksidaan yang rendah bagi ujian pengoksidaan sesuhu dan berkitar. Ini disebabkan terdapatnya laluan resapan ion di dalam sempadan bijian bagi aloi berbijian halus, oleh itu pembentukan pantas lapisan oksida pelindung boleh berlaku. Oleh itu, aloi tersebut boleh digunakan untuk aplikasi suhu tinggi.

## TABLE OF CONTENTS

CHAPTER	TITLE	PAGE
	<b>DECLARATION</b>	ii
	<b>DEDICATION</b>	iii
	<b>ACKNOWLEDGEMENTS</b>	iv
	<b>ABSTRACT</b>	v
	<b>ABSTRAK</b>	vi
	<b>TABLE OF CONTENTS</b>	vii
	<b>LIST OF TABLES</b>	xv
	<b>LIST OF FIGURES</b>	xvi
	<b>LIST OF ABBREVIATIONS</b>	xxxvi
	<b>LIST OF APPENDICES</b>	xxxvii
<b>1</b>	<b>INTRODUCTION</b>	<b>1</b>
	1.1 Introduction	1
	1.2 Background of the Research	6
	1.3 Objective of the Research	7
	1.4 Scope of the Research	8
<b>2</b>	<b>AN OVERVIEW ON FERUM-NICKEL- CHROMIUM ALLOYS</b>	<b>9</b>
	2.1 Introduction	9
	2.2 An Overview of Iron-Nickel-Chromium Alloys	11
	2.2.1 Applications of Iron-Nickel-Chromium Alloys	12

2.2.2	Metallurgy of Iron-Nickel-Chromium Alloys	14
2.2.3	Mechanical Properties of Iron-Nickel-Chromium Alloys	18
2.3	Influence of Heat Treatment on Iron-Nickel-Chromium Alloys	20
<b>3</b>	<b>HIGH TEMPERATURE OXIDATION</b>	<b>26</b>
3.1	Introduction	26
3.2	Mechanisms of High Temperature Oxidation	27
3.2.1	Thermodynamic Considerations	29
3.2.2	Kinetics Considerations	31
3.2.2.1	Rates of Oxidation	32
3.2.2.2	Plotting and Analysis of Rate Data	37
3.2.3	Scale Breakdown	38
3.2.4	Diffusion via Grain Boundary	42
3.3	High Temperature Oxidation of Iron-Nickel-Chromium Alloys	46
3.3.1	Influence of Temperature and Alloying Element on Oxide Scale Morphology of Iron-Nickel-Chromium Alloys	49
3.3.2	Influence of Breakaway Oxidation on Oxide Scale Morphology of Iron-Nickel-Chromium Alloys	58
3.3.3	Influence of Heat Treatment on Oxidation of Iron-Nickel-Chromium Alloys	63
3.4	Summary	72
<b>4</b>	<b>RESEARCH METHODOLOGY</b>	<b>74</b>
4.1	Introduction	74
4.2	Materials	76
4.3	Heat Treatment Process	78
4.3.1	Characterization of Heat Treated Samples	79
4.3.1.1	Optical Microscopy	80

4.3.1.2	Hardness Test	80
4.4	Sample Preparation for Oxidation Tests	81
4.4.1	High Temperature Oxidation Experimental Set-up	82
4.4.1.1	Furnace	84
4.4.1.2	Motorization of the Rig	84
4.5	Oxidation Tests	85
4.5.1	Isothermal Oxidation	86
4.5.2	Cyclic Oxidation	86
4.5.3	Thermogravimetric Analysis in Oxygen	87
4.6	Characterization of Oxidized Samples	88
4.6.1	Scanning Electron Microscopy (SEM)	88
4.6.2	X-Ray Diffraction (XRD)	89
<b>5</b>	<b>RESULTS AND DISCUSSION</b>	<b>90</b>
5.1	Introduction	90
5.2	Materials Before and After Heat Treatment	90
5.2.1	Metallography of As-received and Heat Treated Samples	91
5.2.2	Phase Analysis of As-received and Heat Treated Samples	98
5.2.3	Hardness of As-received and Heat Treated Samples	105
5.3	Isothermal Oxidation of Fe-33Ni-19Cr Alloy	107
5.3.1	Isothermal Oxidation of Fe-33Ni-19Cr Alloy at 500°C	107
5.3.1.1	Oxidation Kinetics of Alloys after Isothermal Oxidation at 500°C	107
5.3.1.2	Phase Identification of Alloys after Isothermal Oxidation at 500°C	113
5.3.1.3	Surface Morphology of Alloys after Isothermal Oxidation at 500°C	115
	a) Oxidation for 300 hours	115



b) Oxidation for 500 hours	117
5.3.1.4 Cross Sectional Analysis of Alloys after Isothermal Oxidation at 500°C	126
5.3.2 Isothermal Oxidation of Fe-33Ni-19Cr Alloy at 700°C	128
5.3.2.1 Oxidation Kinetics of Alloys after Isothermal Oxidation at 700°C	128
5.3.2.2 Phase Identification of Alloys after Isothermal Oxidation at 700°C	131
5.3.2.3 Surface Morphology of Alloys after Isothermal Oxidation at 700°C	134
a) Oxidation for 150 hours	134
b) Oxidation for 300 hours	136
c) Oxidation for 500 hours	140
5.3.2.4 Cross Sectional Analysis of Alloys after Isothermal Oxidation at 700°C	145
5.3.3 Isothermal Oxidation of Fe-33Ni-19Cr Alloy at 900°C	147
5.3.3.1 Oxidation Kinetics of Alloys after Isothermal Oxidation at 900°C	147
5.3.3.2 Phase Identification of Alloys after Isothermal Oxidation at 900°C	150
5.3.3.3 Surface Morphology of Alloys after Isothermal Oxidation at 900°C	152
a) Oxidation for 100 hours	152
b) Oxidation for 150 hours	156
c) Oxidation for 300 hours	158
d) Oxidation for 500 hours	160
5.3.3.4 Cross Sectional Analysis of Alloys after Isothermal Oxidation at 900°C	168
5.3.4 Summary of Isothermal Oxidation of Fe-33Ni- 19Cr Alloy	174
5.4 Isothermal Oxidation of Fe-40Ni-24Cr Alloy	176

5.4.1 Isothermal Oxidation of Fe-40Ni-24Cr Alloy at 500°C	176
5.4.1.1 Oxidation Kinetics of Alloys after Isothermal Oxidation at 500°C	176
5.4.1.2 Phase Identification of Alloys after Isothermal Oxidation at 500°C	179
5.4.1.3 Surface Morphology of Alloys after Isothermal Oxidation at 500°C	181
a) Oxidation for 300 hours	181
b) Oxidation for 500 hours	184
5.4.1.4 Cross Sectional Analysis of Alloys after Isothermal Oxidation at 500°C	188
5.4.2 Isothermal Oxidation of Fe-40Ni-24Cr Alloy at 700°C	190
5.4.2.1 Oxidation Kinetics of Alloys after Isothermal Oxidation at 700°C	190
5.4.2.2 Phase Identification of Alloys after Isothermal Oxidation at 700°C	193
5.4.2.3 Surface Morphology of Alloys after Isothermal Oxidation at 700°C	196
a) Oxidation for 150 hours	196
b) Oxidation for 300 hours	198
c) Oxidation for 500 hours	200
5.4.2.4 Cross Sectional Analysis of Alloys after Isothermal Oxidation at 700°C	207
5.4.3 Isothermal Oxidation of Isothermal Oxidation at 900°C	209
5.4.3.1 Oxidation Kinetics of Alloys after Isothermal Oxidation at 900°C	209
5.4.3.2 Phase Identification of Alloys after Isothermal Oxidation at 900°C	212
5.4.3.3 Surface Morphology of Alloys after Isothermal Oxidation at 900°C	214

a) Oxidation for 100 hours	214
b) Oxidation for 150 hours	216
c) Oxidation for 300 hours	218
d) Oxidation for 500 hours	221
5.4.3.4 Cross Sectional Analysis of Alloys after Isothermal Oxidation at 900°C	223
5.4.4 Summary of Isothermal Oxidation of Fe-40Ni- 24Cr Alloy	225
5.4.5 Summary of Isothermal Oxidation	227
5.5 Cyclic Oxidation of of Fe-33Ni-19Cr Alloy	229
5.5.1 Cyclic Oxidation of Fe-33Ni-19Cr Alloy at 700°C	229
5.5.1.1 Oxidation Kinetics of Alloys after Cyclic Oxidation at 700°C	229
5.5.1.2 Phase Identification of Alloys after Cyclic Oxidation at 700°C	231
5.5.1.3 Surface Morphology of Alloys after Cyclic Oxidation at 700°C	233
a) Oxidation for 100 cycles	233
b) Oxidation for 150 cycles	235
5.5.1.4 Cross Sectional Analysis of Alloys after Cyclic Oxidation at 700°C	238
5.5.2 Cyclic Oxidation of Fe-33Ni-19Cr Alloy at 900°C	242
5.5.2.1 Oxidation Kinetics of Alloys after Cyclic Oxidation at 900°C	242
5.5.2.2 Phase Identification of Alloys after Cyclic Oxidation at 900°C	244
5.5.2.3 Surface Morphology of Alloys after Cyclic Oxidation at 900°C	246
a) Oxidation for 100 cycles	246
b) Oxidation for 150 cycles	246

5.5.2.4	Cross Sectional Analysis of Alloys after Cyclic Oxidation at 900°C	250
5.5.3	Summary of Cyclic Oxidation of Fe-33Ni-19Cr Alloy	252
5.6	Cyclic Oxidation of Fe-40Ni-24Cr Alloy	252
5.6.1	Cyclic Oxidation of Fe-40Ni-24Cr Alloy at 700°C	253
5.6.1.1	Oxidation Kinetics of Alloys after Cyclic Oxidation at 700°C	253
5.6.1.2	Phase Identification of Alloys after Cyclic Oxidation at 700°C	254
5.6.1.3	Surface Morphology of Alloys after Cyclic Oxidation at 700°C	256
	a) Oxidation for 100 cycles	256
	b) Oxidation for 150 cycles	256
5.6.1.4	Cross Sectional Analysis of Alloys after Cyclic Oxidation at 700°C	260
5.6.2	Cyclic Oxidation of Fe-40Ni-24Cr Alloy at 900°C	263
5.6.2.1	Oxidation Kinetics of Alloys after Cyclic Oxidation at 900°C	263
5.6.2.2	Phase Identification of Alloys after Cyclic Oxidation at 900°C	264
5.6.2.3	Surface Morphology of Alloys after Cyclic Oxidation at 900°C	266
	a) Oxidation for 100 cycles	266
	b) Oxidation for 150 cycles	268
5.6.2.4	Cross Sectional Analysis of Alloys after Cyclic Oxidation at 900°C	270
5.6.3	Summary of Cyclic Oxidation of Fe-40Ni-24Cr Alloy	271
5.7	Isothermal Oxidation in High Purity Oxygen of Fe- 33Ni-19Cr Alloy using Thermogravimetric Analysis	272

5.8	Isothermal Oxidation in High Purity Oxygen of Fe-40Ni-24Cr Alloy using Thermogravimetric Analysis	275
5.9	Summary	278
<b>6</b>	<b>CONCLUSIONS AND RECOMMENDATIONS FOR FUTURE WORK</b>	<b>279</b>
6.1	Conclusions	279
6.2	Recommendations for Future Work	281
	<b>REFERENCES</b>	<b>283</b>
	Appendices A-D	294-303

**LIST OF TABLES**

<b>TABLE NO.</b>	<b>TITLE</b>	<b>PAGE</b>
2.1	Mechanical properties data of alloys 800H and HR-120 [Hayness International, 2008; Special Metals Corporation, 2004a; Chen <i>et al.</i> , 2004]	18
4.1	Chemical compositions in weight percent (wt%) of alloys.	77
4.2	Heat treated and as-received samples	79
5.1	EDX analysis of the as-received Fe-33Ni-19Cr alloy (atomic %).	93
5.2	EDX analysis of the as-received Fe-40Ni-24Cr alloy (atomic %).	96
5.3	Summary of weight change per area of isothermal and cyclic oxidation	278

## LIST OF FIGURES








FIGURE NO.	TITLE	PAGE
2.1	Ternary phase diagram of an isothermal section at 650°C for the iron-chromium-nickel system (Smith and Hashemi, 2006).	15
2.2	Superimposed ternary phase diagram of iron-nickel-chromium near the Fe-rich corner at 1200°C (bold lines) and 800°C (dashed lines) (Yamamoto <i>et al.</i> , 2010).	16
2.3	Microstructure of as-received alloy, (a) alloy 800H (Roy & Virupaksha, 2007) and (b) HR-120 alloy (He <i>et al.</i> , 2002).	17
2.4	Microstructure of the Fe-23Ni-12Cr alloy, solution-treated at (a) 1000°C, (b) 1050°C, (c) 1100°C and (d) 1150°C (Cai <i>et al.</i> , 2003).	21
2.5	XRD spectrum of the Fe-23Ni-12Cr alloy after different solution treatments (Cai <i>et al.</i> , 2003).	21
2.6	Microstructure after different solution treatment of Fe-38Ni alloy (a) 1050°C, (b) 1100°C, (c) 1150°C and (d) 1200°C (Zhang <i>et al.</i> , 2008).	22
2.7	Effect of annealing temperature on properties of INCOLOY alloy 800 (UNS N08800), 800H (UNS N08810) and 800HT (UNS N08811) (Special Metals Corporation, 2004a).	24

3.1	Schematic representations of metal-scale-gas system (Smith and Hashemi, 2006).	28
3.2	Ellingham diagram (Khanna, 2002)	30
3.3	Schematic illustrations of oxide formation and growth phenomena (Kofstad, 1988)	32
3.4	The kinetics of logarithmic oxidation (Kofstad, 1988).	33
3.5	The kinetics of parabolic and linear oxidation (Kofstad, 1988).	34
3.6	Schematic diagram of scale formation according to Wagner's model (Birks <i>et al.</i> , 2006)	35
3.7	Double-logarithmic plot ( $\log x$ versus $\log t$ ) of parabolic and logarithmic oxidation. If such processes take place simultaneously, the overall oxidation may obey an approximate cubic rate ( $x^3 \propto t$ ) (Kofstad, 1988).	38
3.8	Schematic plot of weight change as a function of time for isothermal and cyclic oxidation behavior of the same alloy (Kartono, 2007).	41
3.9	Schematic models for the nucleation and growth of oxide on a metal surface (Kofstad, 1988).	43
3.10	Mechanism of preferential grain boundary attack (Birks <i>et al.</i> , 2006).	44
3.11	Model for the development of microchannels above cavities at the metal-oxide interface or in the oxide scale (Kofstad, 1988).	46
3.12	The crystal structure of metals.	50
3.13	The interstitial voids in close-packed structures.	50
3.14	SEM images of the surface morphologies of oxide layer exposed for 1440 hours (Fulger <i>et al.</i> , 2009).	52
3.15	(a) Cross-sectional SEM image of the sample after 1440 h exposure at 600°C and (b) the corresponding composition profile across the oxide thickness (Fulger <i>et al.</i> , 2009).	52

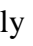



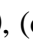











- 3.16 Cross section of oxidized alloy; (a) Fe-17.5Cr-0.45Mn at 800°C, and (b) Fe-22.6Cr-0.44Mn at 650°C (Young *et al.*, 2011). 55
- 3.17 A SEM image of; (a) Ni-19Cr-18Fe-5Nb-3Mo alloy shows Nb-rich precipitates (Tan *et al.*, 2008b), and (b) Ni-22Cr-5Fe-9Mo-4Nb alloy shows a pitting corrosion (Was *et al.*, 2007). 57
- 3.18 (a) SEM BSE image and (b) SEM-EDX analysis of multilayer oxide grown on Fe-20Cr-10Ni at 650°C (Gheno *et al.*, 2012). 59
- 3.19 Schematic representation of nodular oxide growth (Gheno *et al.*, 2012). 61
- 3.20 Schematic illustration showing scale formation of Fe-(9-12%)Cr steels in the temperature range 550-650°C (Saunders *et al.*, 2008). 62
- 3.21 Typical examples of different exposure time on 10Cr-Mo-W steel in Ar-50% $H_2O$ ; (a) 3000 hours, 650°C and (b) 10000 hours, 625°C (Saunders *et al.*, 2008). 63
- 3.22 Cross sectional secondary image and EDX line-scan for ~3 weeks exposed control as-received sample (a,c) and ~4 weeks exposed GBE sample (b,d) (Tan *et al.*, 2006). 66
- 3.23 Volume thermal expansion coefficient ( $\alpha_v$ ) of alloy 800H and oxides such as  $Fe_2O_3$  (hematite),  $Fe_3O_4$  (magnetite),  $FeCr_2O_4$  (spinel), and  $Cr_2O_3$  (eskolaite) (Tan, *et al.*, 2008b; Tan *et al.*, 2008c). 67
- 3.24 Typical morphology of oxide form on alloy Ni-10Fe-29Cr surface (Xu *et al.*, 2012). 68
- 3.25 Temperature dependence of Cr vapour pressure of  $Cr_2O_3$ ,  $FeCr_2O_4$  and  $LaCrO_3$  (Tan *et al.*, 2008b). 70
- 3.26 Morphologies of the samples after aging at 950 °C for: (a) AR-120 h and (b) AR-2000 h (c) GR-120 h and (d) GR-2000 h (Tae *et al.*, 2010). 71

4.1	Research methodology flow chart.	75
4.2	As-received and cut Fe-Ni-Cr samples	78
4.3	Temperature-time profile for heat treatment process.	79
4.4	Prepared samples prior to oxidation test placed in the quartz boat.	81
4.5	Specially built oxidation test rig.	82
4.6	Temperature-time profile for temperature calibration at 700°C. (Temperature difference between furnace and thermocouple is 50°C).	83
4.7	Temperature-distance profile for hot zone region calibration at 700°C.	83
4.8	A schematic diagram showing motor assembly, (a) screw rod, (b) frame attached to furnace, (c) motor.	85
4.9	Temperature-time profile for cyclic oxidation test at 700°C.	87
5.1	Optical micrographs of non-oxidized Fe-33Ni-19Cr alloy, (a) as-received (8HUT), and heat treated for 3 hours (b) 950°C (8H950), (c) 1000°C (8H1000), (d) 1050°C (8H1050), (e) 1100°C (8H1100), (f) 1150°C (8H1150) and (g) 1200°C (8H1200).	92
5.2	SEM image of the as-received Fe-33Ni-19Cr alloy.	93
5.3	Optical micrographs of non-oxidized Fe-40Ni-24Cr alloy, (a) as-received (HRUT), and heat treated for 3 hours (b) 950°C (HR950), (c) 1000°C (HR1000), (d) 1050°C (HR1050), (e) 1100°C (HR1100), (f) 1150°C (HR1150) and (g) 1200°C (HR1200).	95
5.4	SEM image of the as-received Fe-40Ni-24Cr alloy.	96
5.5	Effect of solution treatment on the grain size of Fe-33Ni-19Cr and Fe-40Ni-24Cr alloys	96
5.6	X-ray diffractographs (XRD) of non-oxidized, as-received and heat treated of Fe-33Ni-19Cr alloy.	100
5.7	X-ray diffractographs (XRD) of non-oxidized, as-received and heat treated of Fe-40Ni-24Cr alloy.	103

- 5.8 Effect of solution treatment on the hardness of Fe-33Ni-19Cr and Fe-40Ni-24Cr alloys. 105
- 5.9 Isothermal oxidation kinetics of Fe-33Ni-19Cr alloy at 500°C. 108
- 5.10 Weight change as a function of exposure time of Fe-33Ni-19Cr alloy at 500°C; (a) double log plots indicating parabolic rate law ( $m = 2$ ) and (b) square of weight change indicating  $K_p$  value ( $\text{mg}^2\text{cm}^{-4}\text{s}^{-1}$ ). The fitting parameter  $R^2$  with a value approaching one denotes the increasing consistence of the data with the fitting. 109
- 5.11 A proposed physical model for initial oxide formation for (a) fine grain and (b) coarse grain samples. 112
- 5.12 X-ray diffraction spectrums of Fe-33Ni-19Cr alloy isothermally oxidized at 500°C for 500 hours; (a)  8H950, (b)  8H1000, (c)  8H1050, (d)  8H1100, (e)  8H1150, (f)  8H1200 and (g)  8HUT. 114
- 5.13 Scanning electron micrographs with corresponding EDX spectrum of Fe-33Ni-19Cr alloy isothermally oxidized at 500°C for 50 hours (a-b) and 300 hours (c-h); (a) 8H950, (b) 8H1200, (c) 8H950, (d) 8H950, (e) EDX spectrum of area A, (f) EDX spectrum of spot B, (g) 8H1000 and (h) 8H1050. 116
- 5.14 Scanning electron micrographs of Fe-33Ni-19Cr alloy isothermally oxidized at 500°C for 300 hours; (a) 8H1100, (b) 8H1150, (c) 8H1200 and (d) 8HUT. 117
- 5.15 Scanning electron micrographs with corresponding EDX spectrum of 8H950 samples Fe-33Ni-19Cr alloy isothermally oxidized at 500°C for 500 hours; (a) 8H950 at 10000x, (b) 8H950 at 25000x, (c) EDX spectrum of area C, (d) EDX spectrum of area D and (e) EDX spectrum of area E. 118

- 5.16 A proposed physical model for Ti-rich oxide formation as isolated particles, (a) initial growth, (b) expanded view of (a), (c) lateral growth of the oxide, (d) vertical growth of the oxide and formation of continuous oxide layer. 120
- 5.17 Scanning electron micrographs with corresponding EDX spectrum of 8H1000 samples Fe-33Ni-19Cr alloy isothermally oxidized at 500°C for 500 hours; (a) 8H1000 at 5000x, (b) 8H1000 at 25000x, (c) EDX spectrum of area F, and (d) EDX spectrum of area G. 122
- 5.18 Scanning electron micrographs with corresponding EDX spectrum of Fe-33Ni-19Cr alloy isothermally oxidized at 500°C for 500 hours; (a) 8H1050, (b) EDX spectrum of area H, (c) 8H1100 at 10000x and (d) 8H1100 at 25000x 123
- 5.19 Scanning electron micrographs with corresponding EDX spectrum of Fe-33Ni-19Cr alloy isothermally oxidized at 500°C for 500 hours; (a) 8H1150 at 5000x, (b) 8H1150 at 25000x, (c) 8H1150 at 50000x and (d) EDX spectrum of area I. 124
- 5.20 Scanning electron micrographs with corresponding EDX spectrum of Fe-33Ni-19Cr alloy isothermally oxidized at 500°C for 500 hours; (a) 8H1200 at 10000x, (b) 8H1200 at 25000x, (c) 8HUT at 10000x, (d) 8HUT at 25000x, (e) EDX spectrum of area J and (f) EDX spectrum of area K. 125
- 5.21 Cross sectional scanning electron micrographs of Fe-33Ni-19Cr alloy isothermally oxidized at 500°C for 500 hours; (a) 8H950, (b) EDX spectrum of spot Q, (c) 8H1000 and (d) EDX line scan spectrum of 8H1050. 126






- 5.22 Cross sectional scanning electron micrographs of Fe-33Ni-19Cr alloy isothermally oxidized at 500°C for 500 hours; (a) EDX line scan spectrum of 8H1100, (b) 8H1150, (c) 8H1200 and (d) 8HUT. 127
- 5.23 Isothermal oxidation kinetics of Fe-33Ni-19Cr alloy at 700°C. 129
- 5.24 Weight change as a function of exposure time of Fe-33Ni-19Cr alloy at 700°C; (a) double log plots indicating parabolic rate law ( $m = 2$ ) and (b) square of weight change indicating  $K_p$  value ( $\text{mg}^2\text{cm}^{-4}\text{s}^{-1}$ ). The fitting parameter  $R^2$  with a value approaching one denotes the increasing consistence of the data with the fitting. 130
- 5.25 X-ray diffraction spectrums of Fe-33Ni-19Cr alloy isothermally oxidized at 700°C for 500 hours; (a)  8H950, (b)  8H1000, (c)  8H1050 (d)  8H1100, (e)  8H1150, (f)  8H1200 and (g)  8HUT. 132
- 5.26 Scanning electron micrographs with corresponding EDX spectrum of Fe-33Ni-19Cr alloy isothermally oxidized at 700°C for 150 hours; (a) 8H950, (b) EDX spectrum of area A, (c) 8H1000, (d) 8H1050 (e) 8H1100, (f) 8H1150, (g) 8H1200 and (h) 8HUT. 135
- 5.27 Scanning electron micrographs with corresponding EDX spectrum of Fe-33Ni-19Cr alloy isothermally oxidized at 700°C for 300 hours; (a) 8H950, (b) EDX spectrum of area B, (c) EDX spectrum of area C, (d) 8H1000 (e) 8H1050, (f) 8H1100, (g) EDX spectrum of area D and (h) EDX spectrum of area E. 137
- 5.28 Scanning electron micrographs with corresponding EDX spectrum of Fe-33Ni-19Cr alloy isothermally oxidized at 700°C for 300 hours; (a) 8H1150, (b) EDX spectrum of area F, (c) 8H1200 (1000x), (d) 8H1200 (8000x), (e) EDX spectrum of area G and (f) 8HUT. 139






- 5.29 Scanning electron micrographs with corresponding EDX spectrum of Fe-33Ni-19Cr alloy isothermally oxidized at 700°C for 500 hours; (a) 8H950, (b) EDX spectrum of area H, (c) EDX spectrum of area I, (d) 8H1000, (e) EDX spectrum of area J, (f) EDX spectrum of area K and (g) 8H1050. 141
- 5.30 A proposed physical model for Mn-Cr spinel oxide formation reveal grain boundary oxide. 143
- 5.31 Scanning electron micrographs with corresponding EDX spectrum of Fe-33Ni-19Cr alloy isothermally oxidized at 700°C for 500 hours; (a) 8H1100 (500x), (b) 8H1100 (1000x), (c) 8H1150 (500x), (d) 8H1150 (1000x), (e) 8H1200 (500x), (f) 8H1200 (1000x), (g) EDX spectrum of area L and (h) 8HUT. 144
- 5.32 Cross sectional scanning electron micrographs of Fe-33Ni-19Cr alloy isothermally oxidized at 700°C for 500 hours (EDX line scan: Magnification 2500x); (a) 8H950, (b) 8H950 (10000x), (c) 8H1000, (d) 8H1050, (e) 8H1100, (f) 8H1150, (g) 8H1200 and (h) 8HUT. 146
- 5.33 Isothermal oxidation kinetics of Fe-33Ni-19Cr alloy at 900°C 148
- 5.34 Weight change as a function of exposure time of Fe-33Ni-19Cr alloy at 900°C; (a) double log plots indicating parabolic rate law ( $m = 2$ ) and (b) square of weight change indicating  $K_p$  value ( $\text{mg}^2\text{cm}^{-4}\text{s}^{-1}$ ). The fitting parameter  $R^2$  with a value approaching one denotes the increasing consistence of the data with the fitting. 149
- 5.35 X-ray diffraction spectrums of Fe-33Ni-19Cr alloy isothermally oxidized at 900°C for 500 hours; (a)  8H950, (b)  8H1000, (c)  8H1050, (d)  8H1100, (e)  8H1150, (f)  8H1200 and (g)  8HUT. 151

- 5.36 Scanning electron micrographs of Fe-33Ni-19Cr alloy isothermally oxidized at 900°C for 100 hours; (a) 8H950 (500x), (b) 8H950 (2500x), (c) EDX spectrum of area A, (d) 8H1000, (e) 8H1050 and (f) 8H1100. 153
- 5.37 Scanning electron micrographs with corresponding EDX spectrum of Fe-33Ni-19Cr alloy isothermally oxidized at 900°C for 100 hours; (a) 8H1150, (b) EDX spectrum of area B, (c) EDX spectrum of area C, (d) 8H1200 and (e) 8HUT. 154
- 5.38 A proposed physical model of grain boundary attack produces notch features that would develop the grain boundary oxide topographies under the plan view. 155
- 5.39 Scanning electron micrographs of Fe-33Ni-19Cr alloy isothermally oxidized at 900°C for 150 hours; (a) 8H950, (b) 8H1000, (c) 8H1000 [spherical oxide], (d) 8H1000 [needle-like oxide], (e) 8H1050, (f) 8H1100, (g) 8H1150 (1000x), (h) 8H1150 (10000x), (i) 8H1200 and (j) 8HUT. 156
- 5.40 Scanning electron micrographs of Fe-33Ni-19Cr alloy isothermally oxidized at 900°C for 300 hours; (a) 8H950, (b) 8H1000, (c) 8H1050, (d) 8H1100, (e) 8H1150, (f) 8H1200 (1000x), (g) 8HUT and (h) 8H1200 (3000x). 158
- 5.41 Scanning electron micrographs of Fe-33Ni-19Cr alloy oxidized at 900°C for 300 hours indicate minor oxide spallation; (a,c) 8H1100 and (b,d) 8H1200. 160
- 5.42 Back scattered electron image of scanning electron micrographs of Fe-33Ni-19Cr alloy isothermally oxidized at 900°C for 500 hours; (a) 8H950, (b) 8H1000, (c) 8H1050, (d) 8H1100, (e) 8H1150, (f) 8H1200 (1000x), (g) 8HUT and (h) 8H1200 (3000x). 162






- 5.43 Scanning electron micrographs of Fe-33Ni-19Cr alloy isothermally oxidized at 900°C for 500 hours; (a) 8H950 (500x), (b) 8H950 (10000x) [angular oxide], (c) 8H1000 (500x), (d) 8H1000 (10000x) [angular oxide], (e) 8H1000 (5000x) [spherical oxide], (f) 8H1050 (1000x) and (g) 8H1050 (5000x). 163
- 5.44 Scanning electron micrographs of Fe-33Ni-19Cr alloy isothermally oxidized at 900°C for 500 hours; (a) 8H1100 (100x), (b) 8H1100 (1000x), (c) 8H1100 (5000x) [oxide spalling spot], (d) 8H1150 (100x), (e) 8H1150 (3000x) [oxide spalling spot], (f) 8H1150 (500x), (g) 8H1200 (100x), (h) 8H1200 (500x), (i) 8H1200 (3000x) [oxide spalling spot], (j) 8H1200 (5000x) and (k) 8HUT (1000x). 165
- 5.45 Cross sectional scanning electron micrographs of Fe-33Ni-19Cr alloy oxidized at 900°C for 500 hours (EDX line scan: Magnification 2500x); (a) 8H950, (b) 8H1000, (c) 8H1050, (d) 8H1100, (e) 8H1150, (f) 8H1200 and (g) 8HUT. 168
- 5.46 Cross sectional scanning electron micrographs of Fe-33Ni-19Cr alloy isothermally oxidized at 900°C for 500 hours showing internal oxidation; (a) 8H950, (b) 8H1000, (c) 8H1050, (d) 8H1100, (e) 8H1150, (f) 8H1200 and (g) 8HUT. 172
- 5.47 A proposed physical model of internal oxide penetration into the grain boundary for fine and coarse grain sample. 173
- 5.48 Isothermal oxidation kinetics of fine grain (8H950) and coarse grain (8H1200) Fe-33Ni-24Cr alloy at various oxidation temperature [Full line represent coarse grain and dash line represent fine grain]. 175
- 5.49 Isothermal oxidation kinetics of Fe-40Ni-24Cr alloy at 500°C. 177





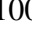

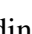
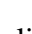

- 5.50 Weight change as a function of exposure time of Fe-40Ni-24Cr alloy at 500°C; (a) double log plots indicating parabolic rate law ( $m = 2$ ) and (b) square of weight change indicating  $K_p$  value ( $\text{mg}^2\text{cm}^{-4}\text{s}^{-1}$ ). The fitting parameter  $R^2$  with a value approaching one denotes the increasing consistence of the data with the fitting. 178
- 5.51 X-ray diffraction spectrums of Fe-40Ni-24Cr alloy isothermally oxidized at 500°C for 500 hours; (a)  HR950, (b)  HR1000, (c)  HR1050, (d)  HR1100, (e)  HR1150, (f)  HR1200 and (g)  HRUT. 180
- 5.52 Scanning electron micrographs with corresponding EDX spectrum of Fe-40Ni-24Cr alloy isothermally oxidized at 500°C for 300 hours; (a) HR950 (500x), (b) HR950 (10000x), (c) EDX spectrum of area A, (d) EDX spectrum of area B, (e) HR1000, (f) HR1050, (g) HR1100, (h) HR1150, (i) HR1200 and (j) HRUT. 182
- 5.53 Scanning electron micrographs with corresponding EDX spectrum of Fe-40Ni-24Cr alloy isothermally oxidized at 500°C for 500 hours; (a) HR950 (1000x), (b) HR950 (10000x), (c) HR950 (50000x), (d) EDX spectrum of area C, (e) EDX spectrum of area D and (f) EDX spectrum of area E. 185
- 5.54 Scanning electron micrographs with corresponding EDX spectrum of Fe-40Ni-24Cr alloy isothermally oxidized at 500°C for 500 hours; (a) HR1000, (b) EDX spectrum of area F, (c) HR1050, (d) EDX spectrum of area G, (e) HR1100 and (f) EDX spectrum of area H. 186






- 5.55 Scanning electron micrographs with corresponding EDX spectrum of Fe-40Ni-24Cr alloy isothermally oxidized at 500°C for 500 hours; (a) HR1150, (b) EDX spectrum of area I, (c) HR1200, (d) EDX spectrum of area J and (e) HRUT. 187
- 5.56 Cross sectional scanning electron micrographs of Fe-40Ni-24Cr alloy isothermally oxidized at 500°C for 500 hours (EDX line scan: Magnification 10000x); (a) HR950, (b) HR1000, (c) HR1050, (d) HR1100, (e) HR1150, (f) HR1200 and (g) HRUT. 189
- 5.57 Isothermal oxidation kinetics of Fe-40Ni-24Cr alloy at 700°C. 191
- 5.58 Weight change as a function of exposure time of Fe-40Ni-24Cr alloy at 700°C; (a) double log plots indicating parabolic rate law ( $m = 2$ ) and (b) square of weight change indicating  $K_p$  value ( $\text{mg}^2\text{cm}^{-4}\text{s}^{-1}$ ). The fitting parameter  $R^2$  with a value approaching one denotes the increasing consistence of the data with the fitting. 192
- 5.59 X-ray diffraction spectrums of Fe-40Ni-24Cr alloy isothermally oxidized at 700°C for 500 hours; (a)  HR950, (b)  HR1000, (c)  HR1050, (d)  HR1100, (e)  HR1150, (f)  HR1200 and (g)  HRUT. 195
- 5.60 Scanning electron micrographs with corresponding EDX spectrum of Fe-40Ni-24Cr alloy isothermally oxidized at 700°C for 150 hours; (a) HR950 (250x), (b) HR950 (2500x), (c) EDX spectrum of area A, (d) HR1000, (e) HR1050 (250x), (f) HR1050 (2500x), (g) EDX spectrum of area B and (h) HR1100. 197






- 5.61 Scanning electron micrographs of Fe-40Ni-24Cr alloy isothermally oxidized at 700°C for 150 hours; (a) HR1150, (b) HR1200, (c) HRUT (500x) and (d) HRUT (10000x). 198
- 5.62 Scanning electron micrographs of Fe-40Ni-24Cr alloy isothermally oxidized at 700°C for 300 hours; (a) HR950, (b) HR1000, (c) HR1050, (d) HR1100, (e) HR1150 and (f) HRUT. 199
- 5.63 Scanning electron micrographs with corresponding EDX spectrum of HR1200 Fe-40Ni-24Cr alloy isothermally oxidized at 700°C for 300 hours; (a) 100x, (b) 3000x, (c) EDX spectrum of area C and (d) EDX spectrum of area D. 200
- 5.64 Scanning electron micrographs with corresponding EDX spectrum of HR950 sample Fe-40Ni-24Cr alloy isothermally oxidized at 700°C for 500 hours; (a) 1000x, (b) rough region (3000x), (c) flat region (3000x), (d) EDX spectrum of area E and (e) EDX spectrum of area F. 201
- 5.65 Scanning electron micrographs with corresponding EDX spectrum of HR1000 sample Fe-40Ni-24Cr alloy isothermally oxidized at 700°C for 500 hours; (a) 100x, (b) 1000x, (c) EDX spectrum of area G and (d) EDX spectrum of area H. 202
- 5.66 Scanning electron micrographs of HR1050 sample Fe-40Ni-24Cr alloy isothermally oxidized at 700°C for 500 hours. 203
- 5.67 Scanning electron micrographs of HR1100 sample Fe-40Ni-24Cr alloy isothermally oxidized at 700°C for 500 hours. 204
- 5.68 Scanning electron micrographs of HR1150 sample Fe-40Ni-24Cr alloy isothermally oxidized at 700°C for 500 hours. 205

- 5.69 Scanning electron micrographs of Fe-40Ni-24Cr alloy isothermally oxidized at 700°C for 500 hours; (a) HR1200 (100x), (b) HR1200 (1000x), (c) HR1200 (500x), (d) HR1200 (3000x), (e) HRUT (100x) and (f) HRUT (1000x). 206
- 5.70 Cross sectional scanning electron micrographs of Fe-40Ni-24Cr alloy oxidized at 700°C for 500 hours (EDX line scan: Magnification 2500x); (a) HR950, (b) HR1000, (c) HR1050, (d) HR1100, (e) HR1150, (f) HR1200 and (g) HRUT. 208
- 5.71 Isothermal oxidation kinetics of Fe-40Ni-24Cr alloy at 900°C. 209
- 5.72 Weight change as a function of exposure time of Fe-40Ni-24Cr alloy at 900°C; (a) double log plots indicating parabolic rate law ( $m = 2$ ) and (b) square of weight change indicating  $K_p$  value ( $\text{mg}^2\text{cm}^{-4}\text{s}^{-1}$ ). The fitting parameter  $R^2$  with a value approaching one denotes the increasing consistence of the data with the fitting. 210
- 5.73 X-ray diffraction spectrums of Fe-40Ni-24Cr alloy isothermally oxidized at 900°C for 500 hours; (a)  HR950, (b)  HR1000, (c)  HR1050, (d)  HR1100, (e)  HR1150, (f)  HR1200 and (g)  HRUT. 213
- 5.74 Scanning electron micrographs of Fe-40Ni-24Cr alloy isothermally oxidized at 900°C for 100 hours indicating minor oxide spallation; (a) HR950, (b) HR1000, (c) HR1050, (d) HR1100, (e) HR1150, (f) HR1200 and (g) HRUT. 215







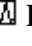
- 5.75 Scanning electron micrographs of Fe-40Ni-24Cr alloy oxidized at 900°C for 150 hours (100x); (a) HR950, (b) HR1000, (c) HR1050, (d) HR1050 (500x), (e) HR1100, (f) HR1100 (500x), (g) HR1150, (h) HR1150 (500x), (i) HR1200 and (j) HRUT. 217
- 5.76 Scanning electron micrographs with corresponding EDX spectrum of Fe-40Ni-24Cr alloy oxidized at 900°C for 300 hours; (a) HR950, (b) HR1000, (c) EDX spectrum of area A, (d) EDX spectrum of area B, (e) HR1050 (500x), (f) HR1050 (3000x), (g) HR1050 (EDX image), (h) EDX spectrum of area C, (i) EDX spectrum of area D, (j) EDX spectrum of area E and (k) EDX spectrum of area F. 219
- 5.77 Scanning electron micrographs of Fe-40Ni-24Cr alloy oxidized at 900°C for 300 hours; (a) HR1100, (b) HR1150, (c) HR1200 and (d) HRUT. 221
- 5.78 Scanning electron micrographs of Fe-40Ni-24Cr alloy oxidized at 900°C for 500 hours; (a) HR950, (b) HR1000, (c) HR1050, (d) HR1100, (e) HR1150, (f) HR1200, (g) HRUT and (h) HR1200 (3000x). 222
- 5.79 Cross sectional scanning electron micrographs of Fe-40Ni-24Cr alloy oxidized at 900°C for 500 hours (EDX line scan: Magnification 5000x); (a) HR950, (b) HR1000, (c) HR1050, (d) HR1100, (e) HR1150, (f) HR1200 and (g) HRUT. 224
- 5.80 Isothermal oxidation kinetics of fine grain (HR950) and coarse grain (HR1200) Fe-40Ni-19Cr alloy [Full line represent coarse grain and dash line represent fine grain]. 226

- 5.81 Isothermal oxidation kinetic of Fe-33Ni-19Cr and Fe-40Ni-24Cr alloy oxidized at: (a) 500°C, (b) 700°C and (c) 900°C. [Full line represent coarse grain, dash line represent fine grain, red colour represent Fe-40Ni-24Cr alloy and blue colour represent Fe-33Ni-24Cr alloy]. 227
- 5.82 Cyclic oxidation kinetics of Fe-33Ni-19Cr alloy at 700°C. 230
- 5.83 X-ray diffraction spectrums of Fe-33Ni-19Cr alloy after cyclic oxidation at 700°C for 150 cycles; (a) , 8H950, (b) , 8H1000, (c) , 8H1050, (d) , 8H1100, (e) , 8H1150, (f) , 8H1200 and (g) , 8HUT. 232
- 5.84 Scanning electron micrographs with corresponding EDX spectrum of Fe-33Ni-19Cr alloy after cyclic oxidation at 700°C for 100 cycles; (a) 8H950 (1000x), (b) EDX spectrum of image (a), (c) 8H1000, (d) 8H1050, (e) 8H1100, (f) 8H1150, (g) 8H1200 and (h) 8HUT. 234
- 5.85 Scanning electron micrographs with corresponding EDX spectrum of Fe-33Ni-19Cr alloy after cyclic oxidation at 700°C for 150 cycles; (a) 8H950 (500x), (b) 8H950 (2500x), (c) EDX spectrum of area A, (d) EDX spectrum of area B, (e) 8H1000 (500x), (f) 8H1000 (2500x), (g) EDX spectrum of area C and (h) EDX spectrum of area D. 236
- 5.86 Scanning electron micrographs with corresponding EDX spectrum of Fe-33Ni-19Cr alloy after cyclic oxidation at 700°C for 150 cycles; (a) 8H1050 (500x), (b) 8H1050 (2500x), (c) EDX spectrum of area E, (d) EDX spectrum of area F, (e) 8H1100 (500x), (f) 8H1100 (2500x), (g) EDX spectrum of area G and (h) EDX spectrum of area H. 237

- 5.87 Scanning electron micrographs with corresponding EDX spectrum of Fe-33Ni-19Cr alloy after cyclic oxidation at 700°C for 150 cycles; (a) 8H1150, (b) 8H1200 and (c) 8HUT. 238
- 5.88 Cross sectional scanning electron micrographs corresponding EDX line scan analysis of Fe-33Ni-19Cr alloy after cyclic oxidation at 700°C for 150 cycles; (a) 8H950, (b) 8H1000, (c) 8H1000 (elemental mapping) and (d) 8H1050. 239
- 5.89 Cross sectional scanning electron micrographs corresponding EDX line scan analysis of Fe-33Ni-19Cr alloy after cyclic oxidation at 700°C for 150 cycles; (a) 8H1100, (b) 8H1150, (c) 8H1200 and (d) 8HUT. 241
- 5.90 Cyclic oxidation kinetics of Fe-33Ni-19Cr alloy at 900°C. 243
- 5.91 X-ray diffraction spectrums of Fe-33Ni-19Cr alloy after cyclic oxidation at 900°C for 150 cycles; (a)  8H950, (b)  8H1000, (c)  8H1050, (d)  8H1100, (e)  8H1150, (f)  8H1200 and (g)  8HUT. 245
- 5.92 Scanning electron micrographs of Fe-33Ni-19Cr alloy after cyclic oxidation at 900°C for 100 cycles; (a) 8H950, (b) 8H1000, (c) 8H1050, (d) 8H1100, (e) 8H1150 (500x), (f) 8H1150 (2500x), (g) 8H1200 and (h) 8HUT. 247
- 5.93 Scanning electron micrographs with corresponding EDX spectrum of Fe-33Ni-19Cr alloy after cyclic oxidation at 900°C for 150 cycles; (a) 8H950, (b) 8H1000, (c) EDX spectrum of area A and (d) EDX spectrum of area B. 248

- 5.94 Scanning electron micrographs with corresponding EDX spectrum of Fe-33Ni-19Cr alloy after cyclic oxidation at 900°C for 150 cycles; (a) 8H1050, (b) 8H1100 (100x), (c) 8H1100 (1000x), (d) 8H1150, (e) 8H1200, (f) 8HUT, (g) EDX spectrum of area C and (h) EDX spectrum of area D. 249
- 5.95 Cross sectional scanning electron micrographs of Fe-33Ni-19Cr alloy after cyclic oxidation at 900°C for 150 cycles (EDX line scan: Magnification 2500x); (a) 8H950, (b) 8H1000, (c) 8H1050, (d) 8H1100, (e) 8H1150, (f) 8H1200 and (g) 8HUT. 251
- 5.96 Cyclic oxidation kinetics of Fe-40Ni-24Cr alloy at 700°C. 254
- 5.97 X-ray diffraction spectrums of Fe-40Ni-24Cr alloy after cyclic oxidation at 700°C for 150 cycles; (a)  HR950, (b)  HR1000, (c)  HR1050, (d)  HR1100, (e)  HR1150, (f)  HR1200 and (g)  HRUT. 255
- 5.98 Scanning electron micrographs of Fe-40Ni-24Cr alloy after cyclic oxidation at 700°C for 100 cycles; (a) 8H950, (b) 8H1000, (c) 8H1050, (d) 8H1100, (e) 8H1150 (f) 8H1200 and (g) 8HUT. 257
- 5.99 Scanning electron micrographs with corresponding EDX spectrum of Fe-40Ni-24Cr alloy after cyclic oxidation at 700°C for 150 cycles; (a) HR950 (1kx), (b) HR950 (10kx), (c) EDX spectrum of area A, (d) EDX spectrum of area B, (e) HR1000 (f) HR1050, (g) HR1100 and (g) HR1150. 258
- 5.100 Scanning electron micrographs with corresponding EDX spectrum of Fe-40Ni-24Cr alloy after cyclic oxidation at 700°C for 150 cycles; (a) HR1200 (250x), (b) HR950 (2500x), (c) EDX spectrum of area C and (d) HRUT. 259



- 5.101 Cross sectional scanning electron micrographs with corresponding EDX line scan analysis of Fe-40Ni-24Cr alloy after cyclic oxidation at 700°C for 150 cycles; (a) HR950, (b) HR1000, (c) HR1050. 261
- 5.102 Cross sectional scanning electron micrographs with corresponding EDX line scan analysis of Fe-40Ni-24Cr alloy after cyclic oxidation at 700°C for 150 cycles; (a) HR1100, (b) HR1150, (c) HR1200 and (d) HRUT. 262
- 5.103 Cyclic oxidation kinetics of Fe-40Ni-24Cr alloy at 900°C 264
- 5.104 X-ray diffraction spectrums of Fe-40Ni-24Cr alloy after cyclic oxidation at 900°C for 150 cycles; (a)  HR950, (b)  HR1000, (c)  HR1050, (d)  HR1100, (e)  HR1150, (f)  HR1200 and (g)  HRUT. 265
- 5.105 Scanning electron micrographs with corresponding EDX spectrum of Fe-40Ni-24Cr alloy after cyclic oxidation at 900°C for 100 cycles; (a) HR950 (1kx), (b) HR950 (5kx), (c) EDX spectrum of area A, (d) EDX spectrum of area B, (e) HR1000 (f) HR1050, (g) HR1100 and (g) EDX spectrum of area C. 267
- 5.106 Scanning electron micrographs of Fe-40Ni-24Cr alloy after cyclic oxidation at 900°C for 100 cycles; (a) HR1150 (250kx), (b) HR1150 (1kx), (c) HR1200 and (d) HRUT 268
- 5.107 Scanning electron micrographs of Fe-40Ni-24Cr alloy after cyclic oxidation 900°C for 150 cycles; (a) HR950, (b) HR1000 (100x), (c) HR1000 (1kx), (d) HR1050, (e) HR1100, (f) HR1150, (g) HR1200 and (h) HRUT. 269

5.108	Cross sectional scanning electron micrographs of Fe-40Ni-24Cr alloy after cyclic oxidation at 900°C for 150 cycles (EDX line scan: Magnification 2500x); (a) HR950, (b) HR1000, (c) HR1050, (d) HR1100, (e) HR1150, (f) HR1200 and (g) HRUT.	270
5.109	Isothermal oxidation kinetics in oxygen of Fe-33Ni-19Cr alloy at 500°C.	273
5.110	Isothermal oxidation kinetics in oxygen of Fe-33Ni-19Cr alloy at 700°C.	274
5.111	Isothermal oxidation kinetics in oxygen of Fe-33Ni-19Cr alloy at 900°C.	275
5.112	Isothermal oxidation kinetics in oxygen of Fe-40Ni-24Cr alloy at 500°C.	276
5.113	Isothermal oxidation kinetics in oxygen of Fe-40Ni-24Cr alloy at 700°C.	277
5.114	Isothermal oxidation kinetics in oxygen of Fe-40Ni-24Cr alloy at 900°C.	277

**LIST OF ABBREVIATIONS**

$\mu\text{m}$	-	micrometer
mm	-	millimeter
cm	-	centimeter
mg	-	milligram
hrs	-	hours
kgf	-	kilogram force
kV	-	kilovolt
mins	-	minutes
$\text{mg}/\text{cm}^2$	-	milligram per centimeter square
$^{\circ}\text{C}$	-	degree Celsius
wt%	-	weight percentage
keV	-	kilo electron volt
rpm	-	revolutions per minute
ml	-	milliliter
ASTM	-	American Society for Testing and Materials
ASME	-	American Society of Mechanical Engineers

**LIST OF APPENDICES**

<b>APPENDIX</b>	<b>TITLE</b>	<b>PAGE</b>
A	List of Publications	294
B	Grain size measurement	296
C	EDX analysis of the isothermally oxidized Fe-33Ni-19Cr alloy at 900°C for 500 hours	298
D	Calculation of weight change per area, $m$ and $K_p$ value.	300

## CHAPTER 1

### INTRODUCTION

#### 1.1 Introduction

Superalloys is an alloy developed for elevated temperature service for extended periods of time with excellent metallurgical stability performance, with combinations of good mechanical properties, good surface stability and high temperature oxidation and corrosion resistant. Superalloys are heat resistant alloys of nickel (Ni), iron (Fe) and cobalt (Co) based alloys that frequently operate at temperature exceeding 540°C. Superalloys are widely used in industrial applications where their high temperature strength and/or oxidation resistance is required. Ni-based superalloys are the most complex of the superalloys and are used in nuclear reactors, gas turbines, petrochemical, aerospace, and heat-treating industries, due to their favourable strength and excellent resistance to oxidation at elevated temperatures (Barnard *et al.*, 2010). Ni-based superalloys has the ability to form protective surface oxide scales at high temperatures that provides them with resistance to further high temperature oxidation (Barnard *et al.*, 2010; Fulger *et al.*, 2009). Based on its advantages, these alloys are widely used in many applications as high temperature structural materials.

Ni-based alloy is characterized by the high phase stability of the face centre cubic austenite matrix. The high content of Ni maintains an austenitic structure to provide structure stability even at room temperature. Ni-based alloy are used for a variety of applications, mainly involved corrosion-resistance and/or heat-resistance. The typical heat-resistance Ni-based alloys are nickel-chromium (Ni-Cr) and iron-nickel-chromium (Fe-Ni-Cr) containing 65 to 80 % Ni and 35 to 70 % Ni respectively. Fe-Ni-Cr alloys are corrosion- and heat-resistant alloys, which are developed for high-temperature oxidizing environments. The Fe-Ni-Cr alloys form a protective surface film of  $\text{Cr}_2\text{O}_3$ , which have excellent corrosion resistance in many severe environments (Campbell, 2008). Oxidation and corrosion resistance is provided by the formation of a protective oxide layer which is formed when the metal is exposed to oxygen and encapsulates the material, and thus protecting the rest of the component. Fe-33Ni-19Cr and Fe-40Ni-24Cr alloys are a standard material of construction for various types of power generation and thermal processing related applications.

In these applications, the components are often subjected to the repeated thermal cyclic, which results a temperature gradient on heating and cooling. A process of heat exchanger in the component involved heat production that affecting materials degradation. Therefore, microstructural stability, oxidation and corrosion resistance behaviour of materials for related applications become a high priority (Pandey *et al.*, 2009; Fulger *et al.*, 2009; Agüero *et al.*, 2005). The key to good corrosion resistance is to establish a continuous layer of a slow growing, thermodynamically stable oxide layer such that subsequent oxidation that are responsible for the protection of metallic alloys in high temperature application (Nie *et al.*, 2010; Peter *et al.*, 2009).

Extensive research has been carried out on oxidation related research on Fe-Ni-Cr alloy for various applications. Fe-33Ni-19Cr and Fe-40Ni-24Cr alloys were selected as promising materials based on studies by various researchers to operate in high temperature conditions. These alloys show a high tendency to form a protective oxide film at high temperatures (Tan *et al.*, 2011a; Nie *et al.*, 2010; Jo *et al.*, 2010).

However, oxide exfoliation was observed as one of a detrimental phenomenon, which may cause obstruction inside the components or severe oxidization damage (Tan *et al.*, 2008b; Iglesias & Raffo Calderon, 2003). One of the possible methods to mitigate the oxide spallation is to introduce compressive stresses at alloys surface, such as shot-peening (Tan *et al.*, 2008b). The metal usually has a higher coefficient of thermal expansion (CTE) than the oxide and induces a compressive stress in the oxide upon cooling (Khanna, 2002). Apparently, introducing the compressive stress at alloy surface would help to reduce the accumulation of strain in the metal-oxide interfaces during cooling. Results on shot-peened sample showed the Cr-rich oxide, spinel and hematite were formed with the absence of magnetite on the refined surface grains improved the oxidation and oxide spallation resistance. This is due to the small difference in CTE volume between the oxides and metal (Tan *et al.*, 2008b). The CTE volume ( $\alpha_v$ ) of hematite and spinel decrease with a similar trend in transitioning from the testing temperature to room temperature, while,  $\alpha_v$  of magnetite becomes significantly different from that of spinel and hematite for temperatures below 400°C. The significant difference in  $\alpha_v$  of magnetite and spinel may have led to the sharper strain change at the spinel-magnetite interface on as-received sample which may cause the exfoliation of oxide scale (Tan *et al.*, 2008c). While the smaller  $\alpha_v$  difference between hematite and spinel may have alleviated the strain at the spinel-hematite interface. Furthermore, hematite has a higher thermal conductivity (12.6 W/m-K) than magnetite (5.0 W/m-K), which more rapidly dissipates heat and results in a higher strain intensity in the outer layer (hematite). The increased strain intensity in hematite further decreased the strain change at the spinel-hematite interface. The strain distribution and the  $\alpha_v$  of the oxides support the experimental observations that the oxide exfoliation occurred mostly at the spinel-magnetite interface.

Thermomechanical treatment of grain boundary engineering also has been extensively investigated to improve the oxidation protection and other properties (Tan *et al.*, 2013; Tan *et al.*, 2011a; Tan & Allen, 2010; Tan *et al.*, 2008a; Tan *et al.*, 2011b; Tan *et al.*, 2006). Whereas, the oxidation behaviour on the effect of grain refinement achieved by heat treatment has never been covered by other researchers.

Additionally, the carbides formation were found to have obvious influences on oxidation rate, which depends on the complex function of matrix structure (Wang *et al.*, 2008). The formation of precipitate at the scale-metal interface and at grain boundary depends on alloying element and working conditions of the oxidized samples (Kochubey *et al.*, 2006). The present of the precipitates may decrease the adherence of the oxide scale to the metallic substrate (Kochubey *et al.*, 2006) and contribute to the preferred site for pit formation (Dutta, 2009; Tan *et al.*, 2008a; Was *et al.*, 2007; Dutta *et al.*, 2004). Whereas, internal oxidation of alloys led to increases the CTE mismatch between the oxides and metal (Hänsel *et al.*, 2003).

The metallurgical factors that influenced the oxidation rate include grain size and alloying elements addition (Deodeshmukh *et al.*, 2011; Fulger *et al.*, 2009; Zurek *et al.*, 2008; Church *et al.*, 2007; Wilson, 1995). Influence of solution treatment temperature on mechanical properties of Fe-Ni-Cr alloy had been reported by Cai *et al.* (2003), and stated that the strength and the ductile properties are affected by different solution treatment and aging. He also observed that microstructure analysis shows different morphologies of precipitation on the matrix and grain boundary with austenitic grains in specimens coarsen, with the increase of solution treatment temperature. Zhang *et al.* (2008) reported that the solution treatments affected the formation of carbides precipitation and the average of grain size of the alloy. The studies revealed that the average grain size increased with increasing the treatment temperature with fewer amounts of carbides found. The solution treatments not only alter the alloy grain structure, but also affect the formation of carbides precipitates in the alloy. Therefore, the solution treatment is one of the possible methods to control the formation of carbides which can hinder the massive decomposition of oxide precipitates.

Grain refinements also affect the internal oxidation (Jo *et al.*, 2010). The grain size is related to internal oxidation at high temperature, specially, smaller grains provide more diffusion paths for alloying elements and oxygen. Studies on Fe-53Ni-22Cr alloy found that oxidized samples forming  $\text{Cr}_2\text{O}_3$  as an external oxide scale and  $\text{Al}_2\text{O}_3$  as an internal oxide. The average depth of internal oxide formed



along the grain boundary decreases in depth for smaller grain size, because internal oxidation took place mainly along grain boundaries. Influence of grain size on the oxidation behaviour for other metal alloy also has been extensively studied by other researcher (Zheng *et al.*, 2009; Peng *et al.*, 2005; Niu *et al.*, 2003; Perez, 2002; Yang *et al.*, 2001; Perez & Adeva, 1998). Studies had indicated that fine grain size shows better resistance to scale spallation, because of the finer grains increasing the relaxation of the oxide scale stress and improving the adhesion of the oxide layer on the matrix (Zheng *et al.*, 2009; Peng *et al.*, 2005; Niu *et al.*, 2003; Perez, 2002; Yang *et al.*, 2001; Perez & Adeva, 1998).

The commercial Fe-Ni-Cr alloy is a Ni-based alloy widely used for high temperature applications as structural materials. For that reason, the oxidation behavior of alloy has been extensively studied. Fe-33Ni-19Cr and Fe-40Ni-24Cr alloys usually used as steam generator in heat exchanger and heat treating furnace component where the equipment are regularly subjected to repeating start-up and shut down cycles. In addition, certain component would undergo long service times that require a material which need to sustain high temperature service condition. Generally, the oxidized Fe-Ni-Cr alloy often exposed to numerous thermal cycling conditions resulting in lower oxidation resistance. Consequently, the isothermal and cyclic oxidation testing would give better understanding in the materials behavior during high temperature service and different operational conditions.

To mitigate oxide spallation, researchers (Zheng *et al.*, 2009; Tan *et al.*, 2008b; Tan *et al.*, 2006; Niu *et al.*, 2003) has found that surface modification, thermomechanical treatment and grain refinement would give superior effect on reduction of oxidation rate. Solution treatment would give great effect on grain size alteration and controlling the precipitates formation of Fe-Ni-Cr alloy which is believed to serve a better oxidation protection at high temperature condition. However limited literature can be found on grain refinement effect of Fe-33Ni-19Cr and Fe-40Ni-24Cr alloys on the oxidation behaviour. Solution treatment would give significant effect on grain size modification of Fe-Ni-Cr alloy. Thus, research on

effect of different grain size on oxidation behavior was performed in this study to comprehend better understanding on oxidation mechanism.

In order to further understand the mechanisms to mitigate oxide spallation, knowledge on the oxidation reaction related to ion diffusion must be fully investigated. Grain refinement will affect the oxidation rate through grain boundary diffusion instead of lattice diffusion. Grain boundary area act as a pathway for cation diffusion to the alloy surface (Stokes *et al.* 1989; Stott, *et al.*, 1987), which develop rapid protective oxide layer.

Therefore, grain refinement may be another approach to improve the resistance to oxide scale spallation, improve the oxide scale adhesion and reduce the depth of internal oxidation, while precipitation of carbide during heat treatment, will be one of factors that can also improve the oxidation resistance. Based on these observations, research on the effect of various grain sizes by means of solution treatment processes on oxidation behaviour of Fe-33Ni-19Cr and Fe-40Ni-24Cr alloys was carried out to give a better understanding on oxidation mechanism at high temperature condition.

## **1.2 Background of the Research**

Recent researchers (Tan *et al.*, 2011(a); Fulger *et al.*, 2009; Tan *et al.*, 2008b; Tan *et al.*, 2006; Iglesias & Raffo Calderon, 2003) indicate that a Fe-Ni-Cr alloy is one of most promising materials that show a high tendency to form a protective oxide film at high temperatures. However oxide exfoliation may occur when the material is exposed at prolonged high temperatures. The adhesion of oxide may be improved by solution treatment whereby variation in grain size may have an influence on the growth mechanism of oxide scale. A comprehensive understanding

of their behaviour under high temperature oxidation environments needs to be developed, so that the alloys can be used widely at elevated temperatures without failure.

The key issues for the oxidation behavior of Fe-Ni-Cr alloys are:

- (a) The alteration of grain size during heat treatment, which can potentially affect the mechanism and kinetics of oxidation.
- (b) The stabilities of oxide scale formation during oxidation, which can improve scale adhesion and mitigate scale exfoliation that will form a protective oxide layer on the metallic surface.

### **1.3 Objective of the Research**

There are three main objective of this research, which are:

- (a) To investigate the mechanism of oxidation on solution treated and as-received samples of Fe-33Ni-19Cr and Fe-40Ni-24Cr alloys at high temperatures.
- (b) To determine the kinetics of oxidation on solution treated and as-received samples of Fe-33Ni-19Cr and Fe-40Ni-24Cr alloys at high temperatures.
- (c) To characterize the oxide scales formed on solution treated and as-received samples of Fe-33Ni-19Cr and Fe-40Ni-24Cr alloys based on qualitative and quantitative analysis.

## 1.4 Scope of the Research

The scopes of this research are:

- (a) Studying the effect of solution treatment process on Fe-33Ni-19Cr and Fe-40Ni-24Cr alloys at various solution treatment temperatures, namely 950°C, 1000°C, 1050°C, 1100°C, 1150°C and 1200°C in order to vary the grain size of the alloys.
- (b) Determining the oxidation kinetics of solution treated and as-received samples of Fe-33Ni-19Cr and Fe-40Ni-24Cr alloys at different conditions (isothermal and cyclic oxidation) and temperatures (500°C, 700°C and 900°C) in a specially built furnace.
- (c) Determining the oxidation kinetics in oxidizing environment of solution treated and as-received samples of Fe-33Ni-19Cr and Fe-40Ni-24Cr alloys under isothermal oxidation condition at different temperatures (500°C, 700°C and 900°C) in high purity oxygen by using Thermogravimetric Analysis (TGA).
- (d) Investigating the properties and morphologies of the oxide scales formed at different oxidizing temperatures using scanning electron microscopy (SEM) technique.
- (e) Investigating the composition of the oxide scale formed on the surface of the materials using x-ray diffraction (XRD) and energy dispersive x-ray (EDX) techniques.

## REFERENCES

- Agüero, A., Raúl, M., Ana, P., and Steve, O. (2005). Long Exposure Steam Oxidation Testing and Mechanical Properties of Slurry Aluminide Coatings for Steam Turbine Components. *Surface and Coatings Technology* 200 (5-6): 1219–1224.
- Allen, T. R., Cole, J. I., Trybus, C. L. and Porter, D. L. (2000). The Effects of Long-Time Irradiation and Thermal Aging on 304 Stainless Steel. *Journal of Nuclear Materials* 282: 171-179.
- Allen, T. R., Tan, L., Was, G. S. and Kenik, E. A. (2007). Thermal and Radiation-Induced Segregation in Model Ni-Base Alloys. *Journal of Nuclear Materials* 361 (2-3): 174–183.
- Allen, T. R., Was, G. S. and Kenik, E. A. (1997). The Effect of Alloy Composition on Radiation-Induced Segregation in Fe-Cr-Ni Alloys. *Journal of Nuclear Materials* 244: 278–294.
- Barnard, B. R., Liaw, P. K., Buchanan, R. A. and Klarstrom, D. L. (2010). Affects of Applied Stresses on the Isothermal and Cyclic High-Temperature Oxidation Behavior of Superalloys. *Materials Science and Engineering: A* 527 (16-17): 3813–3821.
- Bhaduri, A. K., Srinivasan, G., Gill, T. P. S. and Mannan, S. L. (1995). Effect of Aging on the Microstructure and Tensile Properties of an Alloy 800/9Cr-1Mo Steel Joint. *International Journal of Pressure Vessels and Piping* 61 (1): 25–33.
- Birks, N., Meier, G. H. and Pettit, F. S. (2006). *Introduction to the High-Temperature Oxidation of Metals*. (2nd ed.). United Kingdom: Cambridge University Press.
- Borjali, S., Saeed, R., Allahkaram, and Hamed, K. (2012). Effects of Working Temperature and Carbon Diffusion on the Microstructure of High Pressure Heat-Resistant Stainless Steel Tubes Used in Pyrolysis Furnaces during Service Condition. *Materials & Design* 34: 65–73.

- Brünger, E., Wang, X. and Gottstein, G. (1998). Nucleation Mechanisms of Dynamic Recrystallization in Austenitic Steel Alloy 800H. *Scripta Materialia* 38 (12): 1843–1849.
- Cai, D., Mei, Y., Pulin, N. and Wenchang, L. (2003). Influence of Solution Treatment Temperature on Mechanical Properties of a Fe–Ni–Cr Alloy. *Materials Letters* 57 (24-25): 3805–3809.
- Callister, W. D. (2000). *Materials Science and Engineering: An introduction*. (5th ed.) New York: John Wiley & Sons, Inc.
- Campbell, F. C. (2008). *Elements of Metallurgy and Engineering Alloys*. Ohio: ASM International.
- Campbell, F. C. (2006). *Manufacturing Technology for Aerospace Structural Materials*. Elsevier Ltd.
- Cao, G., Firouzdor, V., Sridharan, K., Anderson, M. and Allen, T. R. (2012). Corrosion of Austenitic Alloys in High Temperature Supercritical Carbon Dioxide. *Corrosion Science* 60: 246–255.
- Cao, Y., Di, H., Zhang, J., Zhang, J., Ma, T. and Misra, R. D. K. (2013). An Electron Backscattered Diffraction Study on the Dynamic Recrystallization Behavior of a Nickel–chromium Alloy (800H) during Hot Deformation. *Materials Science and Engineering: A* 585: 71–85.
- Chen, L. J., Liaw, P. K., Wang, H., He, Y. H., McDaniels, R. L., Jiang, L., Yang, B. and Klarstrom, D. L. (2004). Cyclic Deformation Behavior of HAYNES® HR-120® Superalloy under Low-Cycle Fatigue Loading. *Mechanics of Materials* 36 (1-2): 85–98.
- Church, B.C., Sanders, T. H., Speyer, R. F. and Cochran, J. K. (2007). Thermal Expansion Matching and Oxidation Resistance of Fe–Ni–Cr Interconnect Alloys. *Materials Science and Engineering: A* 452-453: 334–340.
- Cubicciotti, D. (1993). Potential-pH diagrams for alloy-water systems under LWR conditions. *Journal of Nuclear Material* 201: 176–183.
- Cullity, B. D. and Stock, S. R. (2001). *Elements of X-Ray Diffraction*. (3rd ed.). New Jersey: Prentice Hall.
- Damborenea, J. D., Lopez, V. and Vázquez, A. J. (1994). Improving High-Temperature Oxidation of Incoloy 800H by Laser Cladding. *Surface and Coatings Technology* 70: 107-113.
- Damcott, D. L., Allen, T. R. and Was, G. S. (1995). Dependence of Radiation-Induced Segregation on Dose, Temperature and Alloy Composition in Austenitic Alloys. *Journal of Nuclear Materials* 225: 97–107.

- De Almeida, Henrique, L., Ribeiro, A. F. and May, I. L. (2002). Microstructural Characterization of Modified 25Cr–35Ni Centrifugally Cast Steel Furnace Tubes. *Materials Characterization* 49 (3): 219–229.
- Dehmlaei, R., Shamanian, M. and Kermanpur, A. (2008). Microstructural Characterization of Dissimilar Welds between Alloy 800 and HP Heat-Resistant Steel. *Materials Characterization* 59 (10): 1447–1454.
- Deodeshmukh, V. P., Matthews, S. J. and Klarstrom, D. L. (2011). High-Temperature Oxidation Performance of a New Alumina-Forming Ni–Fe–Cr–Al Alloy in Flowing Air. *International Journal of Hydrogen Energy* 36 (7): 4580–4587.
- Desnenko, V. A. and Fertman, E. L. (2001). Low Temperature Magnetic Sensor Based on the Age-Hardenable Fe–Cr–Ni Alloy. *Sensors and Actuators A: Physical* 91 (1-2): 120–122.
- Duffaut, F. (1966). Communication Potentiostatic Study of Structural Modofocations Caused in a Ni–Cr–Fe Alloy Heat Treatment at 650°C. *Corrosion Science* (6): 83–85.
- Dutta, R. S. (2009). Corrosion Aspects of Ni–Cr–Fe Based and Ni–Cu Based Steam Generator Tube Materials. *Journal of Nuclear Materials* 393 (2): 343–349.
- Dutta, R. S., Purandare, R., Lobo, A., Kulkarni, S. K. and Dey, G. K. (2004). Microstructural Aspects of the Corrosion of Alloy 800. *Corrosion Science* 46 (12): 2937–2953.
- Ehrlich, K., Konys, J. and Heikinheimo, L. (2004). Materials for High Performance Light Water Reactors. *Journal of Nuclear Materials* 327 (2-3): 140–147.
- Fernandes, C.M., Popovich, V., Matos, M., Senos, A. M. R. and Vieira, M. T. (2009). Carbide Phases Formed in WC–M (M=Fe/Ni/Cr) Systems. *Ceramics International* 35 (1): 369–372.
- Frommert, M., and Gottstein, G. (2009). Mechanical Behavior and Microstructure Evolution during Steady-State Dynamic Recrystallization in the Austenitic Steel 800H. *Materials Science and Engineering: A* 506 (1-2): 101–110.
- Fulger, M., Ohai, D., Mihalache, M., Pantiru, M. and Malinovski, V.. (2009). Oxidation Behavior of Incoloy 800 under Simulated Supercritical Water Conditions. *Journal of Nuclear Materials* 385 (2): 288–293. d
- Geng, S., Qi, S., Zhao, Q., Ma, Z., Zhu, S. and Wang, F. (2012). Effect of Columnar Nano-Grain Structure on the Oxidation Behavior of Low-Cr Fe–Co–Ni Base Alloy in Air at 800°C. *Materials Letters* 80: 33–36.
- Gheno, T., Monceau, D. and Young, D. J. (2012). Mechanism of Breakaway Oxidation of Fe–Cr and Fe–Cr–Ni Alloys in Dry and Wet Carbon Dioxide. *Corrosion Science* 64: 222–233.

- Gottstein, G., Frommert, M., Goerdeler, M. and Schäfer, N. (2004). Prediction of the Critical Conditions for Dynamic Recrystallization in the Austenitic Steel 800H. *Materials Science and Engineering: A* 387-389: 604–608.
- Hänsel, M., Boddington, C. A. and Young, D. J. (2003). Internal Oxidation and Carburisation of Heat-Resistant Alloys. *Corrosion Science* 45 (5): 967–981.
- HAYNES International (2008). *HAYNES® HR-120® alloy*. (H-3125D). U.S.A: Haynes International.
- He, Y., Chen, L., Liaw, P., Mcdaniels, R., Brooks, C., Seeley, R. and Klarstrom, D. (2002). Low-Cycle Fatigue Behavior of HAYNES® HR-120® Alloy. *International Journal of Fatigue* 24 (9): 931–942.
- Holcomb, G. R., and Alman, D. E. (2006). The Effect of Manganese Additions on the Reactive Evaporation of Chromium in Ni–Cr Alloys. *Scripta Materialia* 54 (10): 1821–1825.
- Hur, D. H., Lee, D. H., Choi, M. S., Song, M. H. and Han, J. H. (2008). Root Causes of Intergranular Attack in an Operating Nuclear Steam Generator Tube. *Journal of Nuclear Materials* 375 (3): 382–387.
- Iglesias, A. M. and Raffo Calderon, M. (2003). Thermal Resistance Contributions of Oxides Growth on Incoloy 800 Steam Generator Tubes. *Nuclear Engineering and Design* 219 (1): 1–10.
- Inman, I. A. and Datta, P. S. (2010). Studies of High Temperature Sliding Wear of Metallic Dissimilar Interfaces III: Incoloy MA956 versus Incoloy 800HT. *Tribology International* 43 (11): 2051–2071.
- Jo, T. S., Kim, S. H., Kim, D. G., Park, J. Y. and Kim, Y. D. (2010). Effects of Grain Refinement on Internal Oxidation of Alloy 617. *Journal of Nuclear Materials* 402 (2-3): 162–166.
- Kartono, R. (2007). Effect of platinum, iridium and hafnium to nickel-aluminium alloys under cyclic oxidation conditions. Doctor Philosophy. University of New South Wales.
- Kaya, A. A., Krauklis, P. and Young, D. J. (2002). Microstructure of HK40 Alloy after High Temperature Service in Oxidizing / Carburizing Environment I . Oxidation Phenomena and Propagation of a Crack. *Materials Characterization* 49: 11–21.
- Kelly, J. D. and Wilson, J. C. (1995). Oxidation Rates of Some Heat Resistant Alloys. *Proceedings of the 2nd International Conference on Heat-Resistant Materials*. 11-14 September. Gatlinburg, Tennessee: 53-60.
- Khanna, A. S. (2002). *Introduction to High Temperature Oxidation and Corrosion*. Ohio: ASM International®.



- Khanna, A. S. (2002). *High Temperature Oxidation*. Corrosion Science and Engineering, Indian Institute of Technology, Bombay India.
- Kim, I. S., Hong, J. K., Kim, H. N. and Jang, K. S. (2003). Wear Behavior of Steam Generator Tubes in Nuclear Power Plant Operating Condition. *Proceedings of the 17th International Conference on Structural Mechanics in Reactor Technology*. 17-22 August. Pragues, Czech Republic: 1–7.
- Klarstrom, D. L., Pike, L. M. and Ishwar, V. R. (2013). Nickel-Base Alloy Solutions for Ultrasupercritical Steam Power Plants. *Procedia Engineering* 55: 221–225.
- Klein, L., Bartenwerffer, B. V., Killian, M. S., Schmuki, P. and Virtanen, S.. (2014). The Effect of Grain Boundaries on High Temperature Oxidation of New  $\Gamma'$ -Strengthened Co–Al–W–B Superalloys. *Corrosion Science* 79: 29–33.
- Klueh, R. L. and Nelson, A. T. (2007). Ferritic/martensitic Steels for next-Generation Reactors. *Journal of Nuclear Materials* 371 (1-3): 37–52.
- Kochubey, V., Naumenko, D., Wessel, E., Le Coze, J., Singheiser, L., Al-Badairy, H., Tatlock, G. J. and Quadackers, W. J. (2006). Evidence for Cr-Carbide Formation at the Scale/metal Interface during Oxidation of FeCrAl Alloys. *Materials Letters* 60 (13-14): 1654–1658.
- Kofstad, P. (1988). *High Temperature Corrosion*. London: Elsevier Applied Science.
- Konosu, S., Sakaba, N. and Kaneko, T. (1995). Effects of Heat Treatment on the Creep Crack Growth of Alloy 800H Possessing Long Service History. *Engineering Failure Analysis* 2 (3): 209–214.
- Kumar, M., Schwartz, A. J. and King, W. E. (2002). Microstructural Evolution during Grain Boundary Engineering of Low to Medium Stacking Fault Energy Fcc Materials. *Acta Materialia* 50 (10): 2599–2612.
- Lee, Y. H., Kim, H. K., Kim, H. D., Park, C. Y. and Kim, I. S. (2003). A Comparative Study on the Fretting Wear of Steam Generator Tubes in Korean Power Plants. *Wear* 255 (7-12): 1198–1208.
- Marucco, A. (1995). Phase Transformations during Long-Term Ageing of Ni-Fe-Cr Alloys in the Temperature Range 450–600 °C. *Materials Science and Engineering: A* 194 (2): 225–233.
- Miller, M. K., Anderson, I. M., Bentley, J. and Russell, K. F. (1996). Phase Separation in the Fe-Cr-Ni System. *Applied Surface Science* 94-95: 391–397.
- Nanstad, R. K., McClintock, D. A., Hoelzer, D. T., Tan, L. and Allen, T. R. (2009). High Temperature Irradiation Effects in Selected Generation IV Structural Alloys. *Journal of Nuclear Materials* 392 (2): 331–340.

- Natesan, K. and Shankar, P. S. (2009). Uniaxial Creep Response of Alloy 800H in Impure Helium and in Low Oxygen Potential Environments for Nuclear Reactor Applications. *Journal of Nuclear Materials* 394 (1): 46–51.
- Nie, S. H., Chen, Y., Ren, X., Sridharan, K. and Allen, T. R. (2010). Corrosion of Alumina-Forming Austenitic Steel Fe–20Ni–14Cr–3Al–0.6Nb–0.1Ti in Supercritical Water. *Journal of Nuclear Materials* 399 (2-3): 231–235.
- Niu, Y., Cao, Z. Q., Gesmundo, F., Farnè, G., Randi, G. and Wang, C. L. (2003). Grain Size Effects on the Oxidation of Two Ternary Cu–Ni–20wt.% Cr Alloys at 700–800 °C in 1 Atm O<sub>2</sub>. *Corrosion Science* 45 (6): 1125–1142.
- Oquab, D., Xu, N., Monceau, D. and Young, D. J. (2010). Subsurface Microstructural Changes in a Cast Heat Resisting Alloy Caused by High Temperature Corrosion. *Corrosion Science* 52 (1): 255–262.
- Othman, N. K., Othman, N., Zhang, J. and Young, D. J. (2009). Effects of Water Vapour on Isothermal Oxidation of Chromia-Forming Alloys in Ar/O<sub>2</sub> and Ar/H<sub>2</sub> Atmospheres. *Corrosion Science* 51 (12): 3039–3049.
- Palani, A., Lu, B. T., Tian, L. P., Luo, J. L. and Lu, Y. C. (2010). Effect of Magnesium on the Lead Induced Corrosion and SCC of Alloy 800 in Neutral Crevice Solution at High Temperature. *Journal of Nuclear Materials* 396 (2-3): 189–196.
- Pan, T. J., Li, Y. S., Yang, Q., Feng, R. F. and Hirose, A. (2011). Internal Oxidation and Phase Transformations of Multi-Phase Fe–Ni–Al and Fe–Ni–Al–Cr Alloys Induced by KCl Corrosion. *Corrosion Science* 53 (6): 2115–2121.
- Pandey, M. D., Datla, S., Tapping, R. L. and Lu, Y. C. (2009). The Estimation of Lifetime Distribution of Alloy 800 Steam Generator Tubing. *Nuclear Engineering and Design* 239 (10): 1862–1869.
- Peng, X., Yan, J., Zhou, Y. and Wang, F. (2005). Effect of Grain Refinement on the Resistance of 304 Stainless Steel to Breakaway Oxidation in Wet Air. *Acta Materialia* 53 (19): 5079–5088.
- Perez, P. (2002). Influence of the Alloy Grain Size on the Oxidation Behaviour of PM2000 Alloy. *Corrosion Science* 44: 1793–1808.
- Perez, P., Adeva, P. and Gonzalez, J. L. (1998). Influence of exposure time and grain size on the oxidation behaviour of a PM Ni3Al alloy at 635°C. *Corrosion Science* 40 (4): 631–644.
- Perujo, A., Reimann, J., Feuerstein, H. and Mancinelli, B. (2000). The Oxidation Kinetics of Incoloy 800 and Its Deuterium Permeation Behavior. *Journal of Nuclear Materials* 283-287: 1292–1296.

- Peter, I., Zago, A., Grande, M. A. and Ugues, D. (2009). Thermo-Mechanical and Oxidation Behaviour of High Temperature Advanced Metallic Alloys. *Surface and Coatings Technology* 203 (13): 1776–1784.
- Piekarski, B. (2001). Effect of Nb and Ti Additions on Microstructure, and Identification of Precipitates in Stabilized Ni-Cr Cast Austenitic Steels. *Materials Characterization* 47 (3-4): 181–186.
- Piekarski, B. (2010). The Influence of Nb, Ti, and Si Additions on the Liquidus and Solidus Temperatures and Primary Microstructure Refinement in 0.3C-30Ni-18Cr Cast Steel. *Materials Characterization* 61 (9): 899–906.
- Quadackers, W. J., Khanna, A. S., Schuster, H. and Nickel, H. (1989). Investigation of the Corrosion Mechanisms of Nickel and Nickel-Based Alloys in SO<sub>2</sub>-Containing Environments Using an Evolved Gas Analysis Technique. *Materials Science and Engineering: A* 120-121: 117–122.
- Raman, R. K. S., Khanna, A. S., Choudhary, B. K. and Gnanamoorthy, J. B. (1991). Effect of Thermal Aging on the Oxidation Behaviour of 9wt.%Cr- 1wt.%Mo Steel. *Materials Science and Engineering A* 148: 299–306.
- Ray, A. K., Sinha, S. K., Tiwari, Y. N., Swaminathan, J., Das, G., Chaudhuri, S. and Singh, R. (2003). Analysis of Failed Reformer Tubes. *Engineering Failure Analysis* 10 (3): 351–362.
- Ribeiro, A. F., De Almeida, L. H., Fruchart, D. and Bobrovnichii, G. S. (2003). Microstructural Modifications Induced by Hydrogen in a Heat Resistant Steel Type HP-45 with Nb and Ti Additions. *Journal of Alloys and Compounds* 356-357: 693–696.
- Roy, A. K. and Virupaksha, V. (2007). Performance of Alloy 800H for High-Temperature Heat Exchanger Applications. *Materials Science and Engineering: A* 452-453: 665–672.
- Saunders, S. R. J., Monteiro, M. and Rizzo, F. (2008). The Oxidation Behaviour of Metals and Alloys at High Temperatures in Atmospheres Containing Water Vapour: A Review. *Progress in Materials Science* 53 (5): 775–837.
- Schlegel, S. M., Hopkins, S. and Frary, M. (2009). Effect of Grain Boundary Engineering on Microstructural Stability during Annealing. *Scripta Materialia* 61 (1): 88–91.
- Scott, T. B., Petherbridge, J. R., Harker, N. J., Ball, R. J., Heard, P. J., Glascott, J. and Allen, G. C. (2011). The Oxidative Corrosion of Carbide Inclusions at the Surface of Uranium Metal during Exposure to Water Vapour. *Journal of Hazardous Materials* 195: 115–23.

- Sireesha, M, Albert, S. K. and Sundaresan, S. (2002). Thermal Cycling of Transition Joints between Modified 9Cr–1Mo Steel and Alloy 800 for Steam Generator Application. *International Journal of Pressure Vessels and Piping* 79 (12): 819–827.
- Smart, F. (1983). A Study of the Uptake of Salts from High Pressure Superheated Steam By AISI Type 316 Stainless Steel. *Corrosion Science* 23 (1): 27–39.
- Special Metals Corporation (2004). *INCOLOY<sup>®</sup> alloy 800H & 800HT<sup>®</sup>*. (SMC-047). U.S.A: Special Metals Corporation.
- Stokes, P. S. N., Stott, F. H. and Wood, G. C. (1989). The Influence of Laser Surface Treatment on the High-Temperature Oxidation of Cr<sub>2</sub>O<sub>3</sub>-Forming Alloys. *Materials Science and Engineering A121*: 549–554.
- Stott, F. H. (1992). Developments in Understanding the Mechanisms of Growth of Protective Scales on High-Temperature Alloys. *Materials Characterization* 28 (3): 311–325.
- Stott, F. H., Bartlett, P. K. N. and Wood, G. C. (1987). The Influence of Surface Laser Treatment on the High Temperature Oxidation of Cr<sub>2</sub>O<sub>3</sub>-forming Alloys. *Materials Science and Engineering* 88: 163–169.
- Sun, C., Yang, Y., Liu, Y., Hartwig, K. T., Wang, H. Maloy, S. A., Allen, T. R. and Zhang, X. (2012). Thermal Stability of Ultrafine Grained Fe–Cr–Ni Alloy. *Materials Science and Engineering: A* 542: 64–70.
- Sustaita-Torres, I. A., Rodríguez, S. H., Guerrero-Mata, M. P., Garza, M., Valdés, E., Deschaux-Beaume, F. and Colás, R. (2012). Aging of a Cast 35Cr–45Ni Heat Resistant Alloy. *Materials Chemistry and Physics* 133 (2-3): 1018–1023.
- Szabó, A., Varga, K., Németh, Z., Radó, K., Oravetz, D., Makó, K. E. and Homonnay, Z. (2006). Effect of a Chemical Decontamination Procedure on the Corrosion State of the Heat Exchanger Tubes of Steam Generators. *Corrosion Science* 48 (9): 2727–2749.
- Tan, L., and Allen, T. R.. (2010). Effect of Thermomechanical Treatment on the Corrosion of AA5083. *Corrosion Science* 52 (2): 548–554.
- Tan, L., Allen, T. R. and Busby, J. T.. (2013). Grain Boundary Engineering for Structure Materials of Nuclear Reactors. *Journal of Nuclear Materials* 441 (1-3): 661–666.
- Tan, L., Allen, T. R. and Yang, Y.. (2011). Corrosion Behavior of Alloy 800H (Fe–21Cr–32Ni) in Supercritical Water. *Corrosion Science* 53 (2): 703–711.
- Tan, L., Anderson, M., Taylor, D. and Allen, T. R. (2011). Corrosion of Austenitic and Ferritic-Martensitic Steels Exposed to Supercritical Carbon Dioxide. *Corrosion Science* 53 (10): 3273–3280.

- Tan, L., Busby, J. T., Chichester, H. J. M., Sridharan, K. and Allen, T. R. (2013). Thermomechanical Treatment for Improved Neutron Irradiation Resistance of Austenitic Alloy (Fe–21Cr–32Ni). *Journal of Nuclear Materials* 437 (1-3): 70–74.
- Tan, L., Rakotojaona, L., Allen, T. R., Nanstad, R. K. and Busby, J. T. (2011). Microstructure Optimization of Austenitic Alloy 800H (Fe–21Cr–32Ni). *Materials Science and Engineering: A* 528 (6): 2755–2761.
- Tan, L., Ren, X. and Allen, T. R.. (2010). Corrosion Behavior of 9–12% Cr Ferritic–martensitic Steels in Supercritical Water. *Corrosion Science* 52 (4): 1520–1528.
- Tan, L., Ren, X., Sridharan, K. and Allen, T. R. (2008a). Effect of Shot-Peening on the Oxidation of Alloy 800H Exposed to Supercritical Water and Cyclic Oxidation. *Corrosion Science* 50 (7): 2040–2046.
- Tan, L. (2008b). Corrosion Behavior of Ni-Base Alloys for Advanced High Temperature Water-Cooled Nuclear Plants. *Corrosion Science* 50 (11): 3056–3062.
- Tan, L., Sridharan, K. and Allen, T. R.. (2006). The Effect of Grain Boundary Engineering on the Oxidation Behavior of INCOLOY Alloy 800H in Supercritical Water. *Journal of Nuclear Materials* 348 (3): 263–271.
- Tan, L. (2007). Effect of Thermomechanical Processing on Grain Boundary Character Distribution of a Ni-Based Superalloy. *Journal of Nuclear Materials* 371 (1-3): 171–175.
- Tan, L., Sridharan, K., Allen, T. R., Nanstad, R. K. and McClintock, D. A. (2008). Microstructure Tailoring for Property Improvements by Grain Boundary Engineering. *Journal of Nuclear Materials* 374 (1-2): 270–280.
- Tari, V., Najafizadeh, A., Aghaei, M. H. and Mazloumi, M. A.. (2009). Failure Analysis of Ethylene Cracking Tube. *Journal of Failure Analysis and Prevention* 9 (4): 316–322.
- Voisey, K. T., Liu, Z. and Stott, F. H. (2006). Inhibition of Metal Dusting of Alloy 800H by Laser Surface Melting. *Applied Surface Science* 252 (10): 3658–3666.
- Wang, K., Si, H., Yang, C. and Xu, T. D. (2011). Nonequilibrium Grain Boundary Segregation of Phosphorus in Ni-Cr-Fe Superalloy. *Journal of Iron and Steel Research, International* 18 (1): 61–67.
- Wang, L. M., Wang, Z. B. and Lu, K. (2011). Grain Size Effects on the Austenitization Process in a Nanostructured Ferritic Steel. *Acta Materialia* 59 (9): 3710–3719.
- Wang, S. Q., Wang, F., Cui, X. H. and Chen, K. M.. (2008). Effect of Secondary Carbides on Oxidation Wear of the Cr–Mo–V Cast Steels. *Materials Letters* 62 (2): 279–281.

- Wang, X., Brunger, E. and Gottstein, G. (2002). The Role of Twinning during Dynamic Recrystallization in Alloy 800H. *Scripta Materialia* 46: 875–880.
- Wang, X., Bru, E. and Gottstein, G. (2000). Microstructure Characterization and Dynamic Recrystallization in an Alloy 800H. *Materials Science and Engineering A290*: 180–185.
- Was, G. S., Ampornrat, P., Gupta, G., Teyseyre, S., West, E. A., Allen, T. R. and Sridharan, K. (2007). Corrosion and Stress Corrosion Cracking in Supercritical Water. *Journal of Nuclear Materials* 371 (1-3): 176–201.
- Wright, J. K., Carroll, L. J., Cabet, C., Lillo, T. M., Benz, J. K., Simpson, J. A., Lloyd, W. R., Chapman, J. A. and Wright, R. N. (2012). Characterization of Elevated Temperature Properties of Heat Exchanger and Steam Generator Alloys. *Nuclear Engineering and Design* 251: 252–260.
- Xiao, J., Prud'homme, N., Li, N. and Ji, V. (2013). Influence of Humidity on High Temperature Oxidation of Inconel 600 Alloy: Oxide Layers and Residual Stress Study. *Applied Surface Science* 284: 446–452.
- Xu, P., Zhao, L. Y., Sridharan, K. and Allen, T. R.. (2012). Oxidation Behavior of Grain Boundary Engineered Alloy 690 in Supercritical Water Environment. *Journal of Nuclear Materials* 422 (1-3): 143–151.
- Yamamoto, Y., Brady, M. P., Santella, M. L., Bei, H., Maziasz, P. J. and Pint, B. A. (2010). Overview of Strategies for High-Temperature Creep and Oxidation Resistance of Alumina-Forming Austenitic Stainless Steels. *Metallurgical and Materials Transactions A* 42 (4): 922–931.
- Yamamoto, Y., Takeyama, M., Lu, Z. P., Liu, C. T., Evans, N. D., Maziasz, P. J. and Brady, M. P. (2008). Alloying Effects on Creep and Oxidation Resistance of Austenitic Stainless Steel Alloys Employing Intermetallic Precipitates. *Intermetallics* 16 (3): 453–462.
- Yang, S., Wang, F. and Wu, W. (2001). Effect of Microcrystallization on the Cyclic Oxidation Behavior of B -NiAl Intermetallics at 1000 C in Air. *Intermetallics* 9: 741–744.
- Yang, Z., Xia, G., Walker, M., Wang, C., Stevenson, J. and Singh, P. (2007). High Temperature Oxidation/corrosion Behavior of Metals and Alloys under a Hydrogen Gradient. *International Journal of Hydrogen Energy* 32 (16): 3770–3777.
- Young, D. J., Zurek, J., Singheiser, L and Quadackers, W. J. (2011). Temperature Dependence of Oxide Scale Formation on High-Cr Ferritic Steels in Ar–H<sub>2</sub>–H<sub>2</sub>O. *Corrosion Science* 53 (6): 2131–2141.
- Young, D. J. (2007). *High Temperature Oxidation and Corrosion of Metal*. Elsevier.

- Zhang, J. F., Tu, Y. F., Xu, J., Zhang, J. S. and Zhang, J. L. (2008). Effect of Solid Solution Treatment on Microstructure of Fe-Ni Based High Strength Low Thermal Expansion Alloy. *Journal of Iron and Steel Research, International* 15 (1): 75–78.
- Zheng, H. Z., Lu, S. Q. and Huang, Y. (2009). Influence of Grain Size on the Oxidation Behavior of NbCr<sub>2</sub> Alloys at 950–1200°C. *Corrosion Science* 51 (2): 434–438.
- Zhua, S. M., Wang, L., Li, G. B. and Tjongb, S. C. (1995). Laser Surface Alloying of Incoloy 800H with Silicon Carbide : Microstructural Aspects. *Materials Science and Engineering A201*: 5–7.
- Zurek, J., Young, D. J., Essuman, E., Hänsel, M., Penkalla, H. J., Niewolak, L. and Quadackers, W. J. (2008). Growth and Adherence of Chromia Based Surface Scales on Ni-Base Alloys in High- and Low-pO<sub>2</sub> Gases. *Materials Science and Engineering: A* 477 (1-2): 259–270.